Measurement of branching fraction and search for *CP* violation in $B \to \phi\phi K$

S. Mohanty,[72,80] A. B. Kaliyar,[72] V. Gaur,[81] G. B. Mohanty,[72] I. Adachi,[15,11] K. Adamczyk,[54] H. Aihara,[77] S. Al Said,[71,34] D. M. Asner,[3] H. Atmacan,[7] V. Aulchenko,[4,56] T. Aushev,[17] T. Aziz,[72] V. Babu,[8] S. Bahinipati,[21] P. Behera,[23] M. Bessner,[14] V. Bhardwaj,[20] T. Bilka,[5] J. Biswal,[31] A. Bobrov,[4,56] A. Bozek,[54] M. Bračko,[44,31] T. E. Browder,[14] M. Campajola,[28,49] D. Červenkov,[5] V. Chekelian,[45] A. Chen,[51] B. G. Cheon,[13] K. Chilikin,[40] K. Cho,[36] S.-J. Cho,[84] S.-K. Choi,[12] Y. Choi,[69] S. Choudhury,[22] D. Cinabro,[82] S. Cunliffe,[8] S. Das,[43] N. Dash,[23] G. De Nardo,[28,49] R. Dhamija,[22] F. Di Capua,[28,49] Z. Doležal,[5] T. V. Dong,[10] S. Eidelman,[4,56,40] T. Ferber,[8] B. G. Fulsom,[58] N. Gabyshev,[4,56] A. Garmash,[4,56] A. Giri,[22] P. Goldenzweig,[32] B. Golob,[41,31] O. Grzymkowska,[54] Y. Guan,[7] K. Gudkova,[4,56] C. Hadjivasiliou,[58] S. Halder,[72] K. Hayasaka,[55] H. Hayashii,[50] W.-S. Hou,[53] C.-L. Hsu,[70] K. Inami,[48] A. Ishikawa,[15,11] R. Itoh,[15,11] M. Iwasaki,[57] W. W. Jacobs,[24] H. B. Jeon,[38] S. Jia,[10] Y. Jin,[77] K. K. Joo,[6] K. H. Kang,[38] G. Karyan,[8] B. H. Kim,[65] C. H. Kim,[13] D. Y. Kim,[68] S. H. Kim,[65] Y.-K. Kim,[84] K. Kinoshita,[7] P. Kodyš,[5] T. Konno,[35] S. Korpar,[44,31] D. Kotchetkov,[14] P. Križan,[41,31] P. Krokovny,[4,56] R. Kulasiri,[33] M. Kumar,[43] R. Kumar,[61] K. Kumara,[82] Y.-J. Kwon,[84] K. Lalwani,[43] S. C. Lee,[38] J. Li,[38] L. K. Li,[7] Y. B. Li,[59] L. Li Gioi,[45] J. Libby,[23] Z. Liptak,[14,*] D. Liventsev,[82,15] C. MacQueen,[46] M. Masuda,[76,62] T. Matsuda,[47] M. Merola,[28,49] K. Miyabayashi,[50] R. Mizuk,[40,17] T. J. Moon,[65] R. Mussa,[29] M. Nakao,[15,11] A. Natochii,[14] L. Nayak,[22] M. Nayak,[73] N. K. Nisar,[3] S. Nishida,[15,11] K. Ogawa,[55] S. Ogawa,[74] Y. Onuki,[77] P. Oskin,[40] G. Pakhlova,[17,40] S. Pardi,[28] C. W. Park,[69] H. Park,[38] S.-H. Park,[84] S. Patra,[20] T. K. Pedlar,[42] R. Pestotnik,[31] L. E. Piilonen,[81] T. Podobnik,[41,31] V. Popov,[17] E. Prencipe,[18] M. T. Prim,[32] M. Röhrken,[8] A. Rostomyan,[8] N. Rout,[23] G. Russo,[49] D. Sahoo,[72,80] Y. Sakai,[15,11] S. Sandilya,[22] A. Sangal,[7] T. Sanuki,[75] V. Savinov,[60] G. Schnell,[1,19] J. Schueler,[14] C. Schwanda,[26] A. J. Schwartz,[7] Y. Seino,[55] K. Senyo,[83] M. E. Sevior,[46] M. Shapkin,[27] C. Sharma,[43] J.-G. Shiu,[53] B. Shwartz,[4,56] F. Simon,[45] E. Solovieva,[40] M. Starič,[31] Z. S. Stottler,[81] J. F. Strube,[58] T. Sumiyoshi,[79] M. Takizawa,[66,16,63] K. Tanida,[30] Y. Tao,[9] F. Tenchini,[8] M. Uchida,[78] Y. Unno,[13] S. Uno,[15,11] Y. Usov,[4,56] S. E. Vahsen,[14] R. Van Tonder,[2] G. Varner,[14] K. E. Varvell,[70] A. Vinokurova,[4,56] V. Vorobyev,[4,56,40] C. H. Wang,[52] E. Wang,[60] M.-Z. Wang,[53] P. Wang,[25] X. L. Wang,[10] S. Watanuki,[39] J. Wiechczynski,[54] E. Won,[37] X. Xu,[67] B. D. Yabsley,[70] W. Yan,[64] H. Ye,[8] J. H. Yin,[37] Z. P. Zhang,[64] V. Zhilich,[4,56] and V. Zhukova[40]

(Belle Collaboration)

[1]*University of the Basque Country UPV/EHU, 48080 Bilbao*
[2]*University of Bonn, 53115 Bonn*
[3]*Brookhaven National Laboratory, Upton, New York 11973*
[4]*Budker Institute of Nuclear Physics SB RAS, Novosibirsk 630090*
[5]*Faculty of Mathematics and Physics, Charles University, 121 16 Prague*
[6]*Chonnam National University, Gwangju 61186*
[7]*University of Cincinnati, Cincinnati, Ohio 45221*
[8]*Deutsches Elektronen—Synchrotron, 22607 Hamburg*
[9]*University of Florida, Gainesville, Florida 32611*
[10]*Key Laboratory of Nuclear Physics and Ion-beam Application (MOE) and Institute of Modern Physics, Fudan University, Shanghai 200443*
[11]*SOKENDAI (The Graduate University for Advanced Studies), Hayama 240-0193*
[12]*Gyeongsang National University, Jinju 52828*
[13]*Department of Physics and Institute of Natural Sciences, Hanyang University, Seoul 04763*
[14]*University of Hawaii, Honolulu, Hawaii 96822*
[15]*High Energy Accelerator Research Organization (KEK), Tsukuba 305-0801*
[16]*J-PARC Branch, KEK Theory Center, High Energy Accelerator Research Organization (KEK), Tsukuba 305-0801*
[17]*Higher School of Economics (HSE), Moscow 101000*
[18]*Forschungszentrum Jülich, 52425 Jülich*
[19]*IKERBASQUE, Basque Foundation for Science, 48013 Bilbao*
[20]*Indian Institute of Science Education and Research Mohali, SAS Nagar, 140306*
[21]*Indian Institute of Technology Bhubaneswar, Satya Nagar 751007*
[22]*Indian Institute of Technology Hyderabad, Telangana 502285*
[23]*Indian Institute of Technology Madras, Chennai 600036*
[24]*Indiana University, Bloomington, Indiana 47408*
[25]*Institute of High Energy Physics, Chinese Academy of Sciences, Beijing 100049*

[26]*Institute of High Energy Physics, Vienna 1050*
[27]*Institute for High Energy Physics, Protvino 142281*
[28]*INFN - Sezione di Napoli, 80126 Napoli*
[29]*INFN - Sezione di Torino, 10125 Torino*
[30]*Advanced Science Research Center, Japan Atomic Energy Agency, Naka 319-1195*
[31]*J. Stefan Institute, 1000 Ljubljana*
[32]*Institut für Experimentelle Teilchenphysik, Karlsruher Institut für Technologie, 76131 Karlsruhe*
[33]*Kennesaw State University, Kennesaw, Georgia 30144*
[34]*Department of Physics, Faculty of Science, King Abdulaziz University, Jeddah 21589*
[35]*Kitasato University, Sagamihara 252-0373*
[36]*Korea Institute of Science and Technology Information, Daejeon 34141*
[37]*Korea University, Seoul 02841*
[38]*Kyungpook National University, Daegu 41566*
[39]*Université Paris-Saclay, CNRS/IN2P3, IJCLab, 91405 Orsay*
[40]*P.N. Lebedev Physical Institute of the Russian Academy of Sciences, Moscow 119991*
[41]*Faculty of Mathematics and Physics, University of Ljubljana, 1000 Ljubljana*
[42]*Luther College, Decorah, Iowa 52101*
[43]*Malaviya National Institute of Technology Jaipur, Jaipur 302017*
[44]*University of Maribor, 2000 Maribor*
[45]*Max-Planck-Institut für Physik, 80805 München*
[46]*School of Physics, University of Melbourne, Victoria 3010*
[47]*University of Miyazaki, Miyazaki 889-2192*
[48]*Graduate School of Science, Nagoya University, Nagoya 464-8602*
[49]*Università di Napoli Federico II, 80126 Napoli*
[50]*Nara Women's University, Nara 630-8506*
[51]*National Central University, Chung-li 32054*
[52]*National United University, Miao Li 36003*
[53]*Department of Physics, National Taiwan University, Taipei 10617*
[54]*H. Niewodniczanski Institute of Nuclear Physics, Krakow 31-342*
[55]*Niigata University, Niigata 950-2181*
[56]*Novosibirsk State University, Novosibirsk 630090*
[57]*Osaka City University, Osaka 558-8585*
[58]*Pacific Northwest National Laboratory, Richland, Washington 99352*
[59]*Peking University, Beijing 100871*
[60]*University of Pittsburgh, Pittsburgh, Pennsylvania 15260*
[61]*Punjab Agricultural University, Ludhiana 141004*
[62]*Research Center for Nuclear Physics, Osaka University, Osaka 567-0047*
[63]*Meson Science Laboratory, Cluster for Pioneering Research, RIKEN, Saitama 351-0198*
[64]*Department of Modern Physics and State Key Laboratory of Particle Detection and Electronics, University of Science and Technology of China, Hefei 230026*
[65]*Seoul National University, Seoul 08826*
[66]*Showa Pharmaceutical University, Tokyo 194-8543*
[67]*Soochow University, Suzhou 215006*
[68]*Soongsil University, Seoul 06978*
[69]*Sungkyunkwan University, Suwon 16419*
[70]*School of Physics, University of Sydney, New South Wales 2006*
[71]*Department of Physics, Faculty of Science, University of Tabuk, Tabuk 71451*
[72]*Tata Institute of Fundamental Research, Mumbai 400005*
[73]*School of Physics and Astronomy, Tel Aviv University, Tel Aviv 69978*
[74]*Toho University, Funabashi 274-8510*
[75]*Department of Physics, Tohoku University, Sendai 980-8578*
[76]*Earthquake Research Institute, University of Tokyo, Tokyo 113-0032*
[77]*Department of Physics, University of Tokyo, Tokyo 113-0033*
[78]*Tokyo Institute of Technology, Tokyo 152-8550*
[79]*Tokyo Metropolitan University, Tokyo 192-0397*
[80]*Utkal University, Bhubaneswar 751004*
[81]*Virginia Polytechnic Institute and State University, Blacksburg, Virginia 24061*
[82]*Wayne State University, Detroit, Michigan 48202*

[83]Yamagata University, Yamagata 990-8560
[84]Yonsei University, Seoul 03722

(Received 20 January 2021; accepted 8 March 2021; published 29 March 2021)

We report the measurement of branching fractions and CP-violation asymmetries in $B \to \phi\phi K$ decays based on a 711 fb^{-1} data sample containing 772×10^6 $B\bar{B}$ events. The data were recorded at the $\Upsilon(4S)$ resonance with the Belle detector at the KEKB asymmetric-energy e^+e^- collider. For $B^+ \to \phi\phi K^+$, the branching fraction and CP-violation asymmetry measured below the η_c threshold ($m_{\phi\phi} < 2.85$ GeV$/c^2$) are $[3.43^{+0.48}_{-0.46}(\text{stat}) \pm 0.22(\text{syst})] \times 10^{-6}$ and $-0.02 \pm 0.11(\text{stat}) \pm 0.01(\text{syst})$, respectively. Similarly, the branching fraction obtained for $B^0 \to \phi\phi K^0$ below the η_c threshold is $[3.02^{+0.75}_{-0.66}(\text{stat}) \pm 0.20(\text{syst})] \times 10^{-6}$. We also measure the CP-violation asymmetry for $B^+ \to \phi\phi K^+$ within the η_c region ($m_{\phi\phi} \in [2.94, 3.02]$ GeV$/c^2$) to be $+0.12 \pm 0.12(\text{stat}) \pm 0.01(\text{syst})$.

DOI: 10.1103/PhysRevD.103.052013

B-meson decays to three-body $\phi\phi K$ final states proceed via a $b \to s\bar{s}s$ loop (penguin) transition, which requires the creation of an additional $s\bar{s}$ pair. The same final state can also originate from the tree-level process $B \to \eta_c(\to \phi\phi)K$. Figure 1 shows the dominant Feynman diagrams that contribute to these decays. The interference between penguin and tree amplitudes is maximal when the $\phi\phi$ invariant mass lies close to the η_c mass ($m_{\phi\phi} \in [2.94, 3.02]$ GeV$/c^2$). No CP violation is expected from this interference, as the relative weak phase between the two amplitudes is $\arg(V_{tb}V_{ts}^*/V_{cb}V_{cs}^*) \approx 0$, where V_{ij} denote CKM matrix elements [1]. A potential new physics (NP) contribution to the loop, however, can introduce a nonzero CP-violating phase. In particular, the CP asymmetry can be as large as 40% in the presence of NP [2]. Thus, an observation of large CP violation in $B \to \phi\phi K$ would indicate the presence of physics beyond the Standard Model. In addition to being an NP probe, the decay is sensitive to the possible production of a glueball candidate near 2.3 GeV$/c^2$ that can subsequently decay to $\phi\phi$ [3]. We can also search for a structure at 2.35 GeV$/c^2$ observed in the $m_{\phi\phi}$ distribution in two-photon collisions [4] and dubbed the $X(2350)$.

Based on a 78 fb^{-1} data sample, Belle reported the first evidence for the decay with a branching fraction $\mathcal{B}(B^+ \to \phi\phi K^+) = [2.6^{+1.1}_{-0.9}(\text{stat}) \pm 0.3(\text{syst})] \times 10^{-6}$ [5] below the η_c threshold ($m_{\phi\phi} < 2.85$ GeV$/c^2$) [6]. The result was consistent with the corresponding theory prediction, which lies in the range $(1.3 - 4.2) \times 10^{-6}$ [7,8]. The *BABAR* experiment performed a measurement of this decay using their full dataset of 464×10^6 $B\bar{B}$ events [9]. The branching fraction obtained with the same $m_{\phi\phi}$ requirement was $\mathcal{B}(B^+ \to \phi\phi K^+) = (5.6 \pm 0.5 \pm 0.3) \times 10^{-6}$, about three standard deviations above Belle's result and larger than theoretical estimates. The $B^0 \to \phi\phi K^0$ channel was observed with a branching fraction of $(4.5 \pm 0.8 \pm 0.3) \times 10^{-6}$. *BABAR* also reported CP asymmetries for charged B decays as $-0.10 \pm 0.08 \pm 0.02$ below the η_c threshold and $+0.09 \pm 0.10 \pm 0.02$ within the η_c region.

In this paper, we update our earlier result [5] with a significantly larger data sample containing 772×10^6 $B\bar{B}$ events. The data were collected at the $\Upsilon(4S)$ resonance with the Belle detector [10] at the KEKB asymmetric-energy e^+e^- collider [11]. The subdetectors relevant for our study are a silicon vertex detector (SVD), a central drift chamber (CDC), an array of aerogel threshold Cherenkov counters (ACC), and time-of-flight scintillation counters (TOF). All these are located inside a 1.5 T axial magnetic field.

To reconstruct $B^+ \to \phi\phi K^+$ and $B^0 \to \phi\phi K^0$ decay candidates, we combine a pair of ϕ mesons with a charged kaon and K_S^0, respectively. All charged tracks except for those from the K_S^0 must have a distance of closest approach with respect to the interaction point (IP) of less than 0.2 cm in the transverse $r - \phi$ plane, and less than 5.0 cm along the z axis. The z axis is defined as the direction opposite that of the e^+ beam. We identify charged kaons based on a likelihood ratio $\mathcal{R}_{K/\pi} = \mathcal{L}_K/(\mathcal{L}_K + \mathcal{L}_\pi)$, where $\mathcal{L}_K$ and $\mathcal{L}_\pi$ denote the individual likelihood for kaons and pions, respectively. These are calculated using specific ionization in the CDC and information from the ACC and the TOF. A requirement $\mathcal{R}_{K/\pi} > 0.6$ is applied to select kaon candidates. The kaon identification efficiency, averaged over the momentum range, is 90%, with a pion misidentification rate of about 10%.

We reconstruct the ϕ candidates from pairs of oppositely charged kaons with an invariant mass in the range 1.00–1.04 GeV$/c^2$, corresponding to $\pm 5\sigma$ (σ is the width

*Now at Hiroshima University.

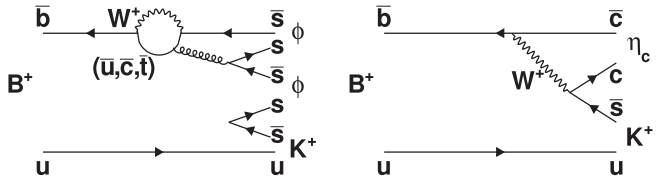

FIG. 1. Dominant Feynman diagrams that contribute to the decays (left) $B^+ \to \phi\phi K^+$ and (right) $B^+ \to \eta_c K^+$. Replacement of the spectator u quark with a d quark will lead to the corresponding diagrams for $B^0 \to \phi\phi K^0$ and $B^0 \to \eta_c K^0$.

of the mass distribution) around the nominal ϕ mass [12]. This is referred to as the M_{KK} signal region in the following discussion. The K_S^0 candidates are reconstructed from two oppositely charged tracks, assumed to be pions, and are further required to satisfy a criterion on the output of a neural network (NN) algorithm [13]. The algorithm uses the following input variables: the K_S^0 momentum in the lab frame; the distance of closest approach along the z axis between the two pion tracks; the flight length in the $r-\phi$ plane; the angle between the K_S^0 momentum and the vector joining the IP to the K_S^0 decay vertex; the angle between the K_S^0 momentum in the lab frame and the pion momentum in the K_S^0 rest frame; the distances of closest approach in the $r-\phi$ plane between the IP and the two pion tracks; the number of CDC hits for each pion track; and the presence or absence of SVD hits for each pion track. We require that the invariant mass lie between 491 MeV/c^2 and 504 MeV/c^2, which corresponds to a $\pm 3\sigma$ window in resolution around the nominal K_S^0 mass [12].

B-meson candidates are identified with two kinematic variables: the beam-energy-constrained mass $M_{\rm bc} \equiv \sqrt{E_{\rm b}^2/c^4 - |\sum_i \vec{p}_i/c|^2}$, and the energy difference $\Delta E \equiv \sum_i E_i - E_{\rm b}$, where $E_{\rm b}$ is the beam energy, and $\vec{p}_i$ and E_i are the momentum and energy, respectively, of the i-th decay product of the B candidate. All these quantities are evaluated in the e^+e^- center-of-mass (CM) frame. We perform a fit for each B candidate, constraining its decay products to originate from a common vertex. Candidate events with $M_{\rm bc} \in [5.230, 5.289]$ GeV/c^2 and $|\Delta E| < 0.1$ GeV are retained for further study. The $M_{\rm bc}$ requirement corresponds to approximately $(-16\sigma, +3\sigma)$ in resolution around the nominal B mass [12], and the ΔE requirement denotes a $\pm 10\sigma$ window around zero. We apply such loose requirements on $M_{\rm bc}$ and ΔE as these are used in a maximum-likelihood fit to obtain the signal yield (described later). We define a signal region as $M_{\rm bc} \in [5.272, 5.289]$ GeV/c^2 and $|\Delta E| < 0.05$ GeV.

After application of the above selection criteria, the average number of B candidates found per event selected in data are 1.7 and 1.6 for $B^+ \to \phi\phi K^+$ and $B^0 \to \phi\phi K^0$, respectively. In the case of multiple B candidates, we choose the candidate with the lowest χ^2 value for the aforementioned B-vertex fit. From Monte Carlo (MC) simulation the best candidate selection method is found to have an efficiency of 68% (65%) to correctly identify the B-meson candidate in $B^+ \to \phi\phi K^+$ ($B^0 \to \phi\phi K^0$) decays. In only about 6% of the total signal events, the B candidate is misreconstructed due to swapping of kaons between the two ϕ candidates, or of one daughter track with that from the rest of the event. Such misreconstructed events are treated as a part of the signal.

The dominant background is from the $e^+e^- \to q\bar{q}$ ($q = u, d, s, c$) continuum process. To suppress this background, observables based on event topology are used. The event shape in the CM frame is expected to be spherical for $B\bar{B}$ events and jetlike for continuum events. We use an NN [13] to combine the following six variables: a Fisher discriminant formed out of 16 modified Fox-Wolfram moments [14]; the cosine of the angle between the B momentum and the z axis; the cosine of the angle between the B thrust axis [15] and the z axis; the cosine of the angle between the thrust axis of the B candidate and that of the rest of the event; the ratio of the second- to the zeroth-order Fox-Wolfram moments (all quantities are calculated in the CM frame); and the vertex separation along the z axis between the B candidate and the remaining tracks. The NN training and validation are performed with signal and $q\bar{q}$ MC simulated events. The signal sample is generated with the EVTGEN program [16], assuming a uniform distribution over the three-body phase space of the final state.

The neural network output ($O_{\rm NN}$) ranges between -1.0 and 1.0, where events near -1.0 (1.0) are more continuum-(signal-)like. We apply a loose criterion $O_{\rm NN} > -0.5$ to reduce the continuum background. The relative signal efficiency loss due to this requirement is about 6% (3%) for $B^+ \to \phi\phi K^+$ ($B^0 \to \phi\phi K^0$) decays, whereas the fraction of continuum events rejected is 76% (66%). As the remainder of the $O_{\rm NN}$ distribution strongly peaks near 1.0 for signal, it is difficult to model with an analytic function. However, the transformed variable

$$O'_{\rm NN} = \log\left[\frac{O_{\rm NN} - O_{\rm NN,min}}{O_{\rm NN,max} - O_{\rm NN}}\right], \tag{1}$$

where $O_{\rm NN,min} = -0.5$ and $O_{\rm NN,max} \simeq 1.0$, has a Gaussian-like distribution that is easier to model. Thus, we use this transformed variable in our signal fit.

Backgrounds due to B decays, mediated by the dominant $b \to c$ transition, are studied with MC samples of such decays. For both $B^+ \to \phi\phi K^+$ and $B^0 \to \phi\phi K^0$ channels, the $M_{\rm bc}$ and ΔE distributions are found to peak in the signal region. To investigate the source of these contributions, we inspect the $m_{\phi\phi}$ distribution, which displays several peaks corresponding to the η_c and other charmonium resonances. To suppress these peaking backgrounds, we exclude candidates for which the $m_{\phi\phi}$ value is greater than 2.85 GeV/c^2. This requirement also allows us to compare our results with the earlier ones from Belle [5] and

BABAR [9]. We calculate the detection efficiencies for candidate events below the η_c threshold to be 12.4% and 12.0% for $B^+ \to \phi\phi K^+$ and $B^0 \to \phi\phi K^0$, respectively.

Charmless backgrounds that do not produce only kaons in the final state may still contribute to the $M_{\rm bc} - \Delta E$ signal region when a final-state particle is misidentified. These are studied with a $B\bar{B}$ MC sample in which one of the B mesons decays via $b \to u, d, s$ transitions with known or estimated branching fractions [12]. Only 40 events survive from an MC sample equivalent to 50 times the size of the data sample. This small component is combined with the events surviving from $b \to c$ transitions to form an overall $B\bar{B}$ background component. In addition to this $B\bar{B}$ background that does not peak in $M_{\rm bc}$ or ΔE, we can have contributions from $B \to \phi KKK$ and $B \to KKKKK$ decays (described later), which have the same final-state particles as the signal.

The signal yield is obtained with an unbinned extended maximum-likelihood fit to the three variables $M_{\rm bc}$, ΔE, and $O'_{\rm NN}$. We define a probability density function (PDF) for each event category, i.e., signal, $q\bar{q}$, and $B\bar{B}$ backgrounds:

$$\mathcal{P}_j^i \equiv \frac{1}{2}(1 - q_i \mathcal{A}_{CP,j})\mathcal{P}_j(M_{\rm bc}^i)\mathcal{P}_j(\Delta E^i)\mathcal{P}_j(O'^i_{\rm NN}), \quad (2)$$

where i denotes the event index, q_i is the charge of the B candidate ($q_i = \pm 1$ for $B^\pm$), and $\mathcal{P}_j$ and $\mathcal{A}_{CP,j}$ are the PDF and CP asymmetry, respectively, for the event category j. The latter is defined as

$$\mathcal{A}_{CP} = \frac{N_{B^-} - N_{B^+}}{N_{B^-} + N_{B^+}}, \quad (3)$$

where N_{B^+} (N_{B^-}) is the number of B^+ (B^-) events. We find equal detection efficiencies for the B^+ ($12.3 \pm 0.1\%$) and B^- ($12.4 \pm 0.1\%$) decays. For neutral B decays, we replace the factor $\frac{1}{2}(1 - q_i \mathcal{A}_{CP,j})$ by 1 in Eq. (2). We also do not perform a CP-violation study in this case, since we would need to tag the recoiling B candidate for that, causing further loss in efficiency on top of the small signal yield. As the correlations among $M_{\rm bc}$, ΔE, and $O'_{\rm NN}$ are found to be small ($\lesssim 5\%$), the product of three individual PDFs is a good approximation for the total PDF. The extended likelihood function is

$$\mathcal{L} = \frac{e^{-\sum_j n_j}}{N!} \prod_i \left[\sum_j n_j \mathcal{P}_j^i \right], \quad (4)$$

where n_j is the yield of event category j, and N is the total number of candidate events. From the fitted signal yield ($n_{\rm sig}$), we calculate the branching fraction as

$$\mathcal{B}(B \to \phi\phi K) = \frac{n_{\rm sig}}{\varepsilon N_{B\bar{B}} [\mathcal{B}(\phi \to K^+K^-)]^2}, \quad (5)$$

TABLE I. List of PDFs used to model the $M_{\rm bc}$, ΔE, and, $O'_{\rm NN}$ distributions for various event categories for $B \to \phi\phi K$. The notation G, AG, 2G, ARG, and Poly1 denote Gaussian, asymmetric Gaussian, sum of two Gaussians, ARGUS [17] function, and first-order polynomial, respectively.

Event category	$M_{\rm bc}$	ΔE	$O'_{\rm NN}$
Signal	G + ARG	2G + Poly1	G + AG
$q\bar{q} + B\bar{B}$	ARG	Poly1	G

where ε and $N_{B\bar{B}}$ are the detection efficiency and the number of $B\bar{B}$ events, respectively. In case of $B^0 \to \phi\phi K^0$, we multiply the denominator by a factor of $\frac{1}{2}$ to account for $K^0 \to K^0_S$, as well as by the subdecay branching fraction $\mathcal{B}(K^0_S \to \pi^+\pi^-)$ [12].

As the expected yield of the nonpeaking $B\bar{B}$ background is small, and it is distributed similarly to $q\bar{q}$ in $M_{\rm bc}$ and ΔE, we merge $q\bar{q}$ and $B\bar{B}$ backgrounds into a single component. We find that the difference in the $O'_{\rm NN}$ distribution between the two backgrounds contributes a negligible systematic uncertainty. Table I lists the PDF shapes used to model $M_{\rm bc}$, ΔE, and $O'_{\rm NN}$ distributions for various event categories of $B \to \phi\phi K$ candidates. The yield and PDF shape parameters of the combined background are floated in $B^+ \to \phi\phi K^+$. For the neutral channel, however, the background PDF shapes are fixed to their MC values after correcting for small differences between data and simulation, as obtained from the charged decay. Similarly, for the signal components, we fix the $M_{\rm bc}$, ΔE, and $O'_{\rm NN}$ shapes to MC values and correct for small data-MC differences according to values obtained from a control sample of $B^+ \to D_s^+ \bar{D}^0$ decays, where $D_s^+ \to \phi(\to K^+K^-)\pi^+$ and $\bar{D}^0 \to K^+\pi^-$.

We apply the above 3D fit to $B^+ \to \phi\phi K^+$ and $B^0 \to \phi\phi K^0$ candidate events to determine the signal yield (and $\mathcal{A}_{CP}$ in the first case). Figures 2 and 3 show $M_{\rm bc}$, ΔE, and $O'_{\rm NN}$ projections of the fits. The fit results are listed in Table II. We find signal yields of $85.0^{+10.2}_{-9.5}$ for $B^+ \to \phi\phi K^+$ and $26.5^{+5.8}_{-5.1}$ for $B^0 \to \phi\phi K^0$, and an $\mathcal{A}_{CP}$ value of -0.02 ± 0.11 for the first case. We also apply the 3D fit to $B^+ \to \phi\phi K^+$ candidate events with $m_{\phi\phi}$ within the η_c region to calculate the signal yield and $\mathcal{A}_{CP}$ value. The corresponding $M_{\rm bc}$ and ΔE projections are shown in Fig. 4, with the fit results listed in Table II. We obtain a signal yield of $73.2^{+9.0}_{-8.3}$ and an $\mathcal{A}_{CP}$ value of $+0.12 \pm 0.12$ in the η_c region. The signal significance is calculated as $\sqrt{-2\log(\mathcal{L}_0/\mathcal{L}_{\rm max})}$, where $\mathcal{L}_0$ and $\mathcal{L}_{\rm max}$ are the likelihood values with the signal yield fixed to zero and for the nominal fit, respectively. We include systematic uncertainties that impact only the signal yield into the likelihood curve via a Gaussian convolution before calculating the final significance.

To estimate the contribution of $B \to \phi KKK$ and $B \to KKKKK$ decays in the M_{KK} signal region (SR), we repeat the 3D fit in the following two sidebands: SB1 is denoted

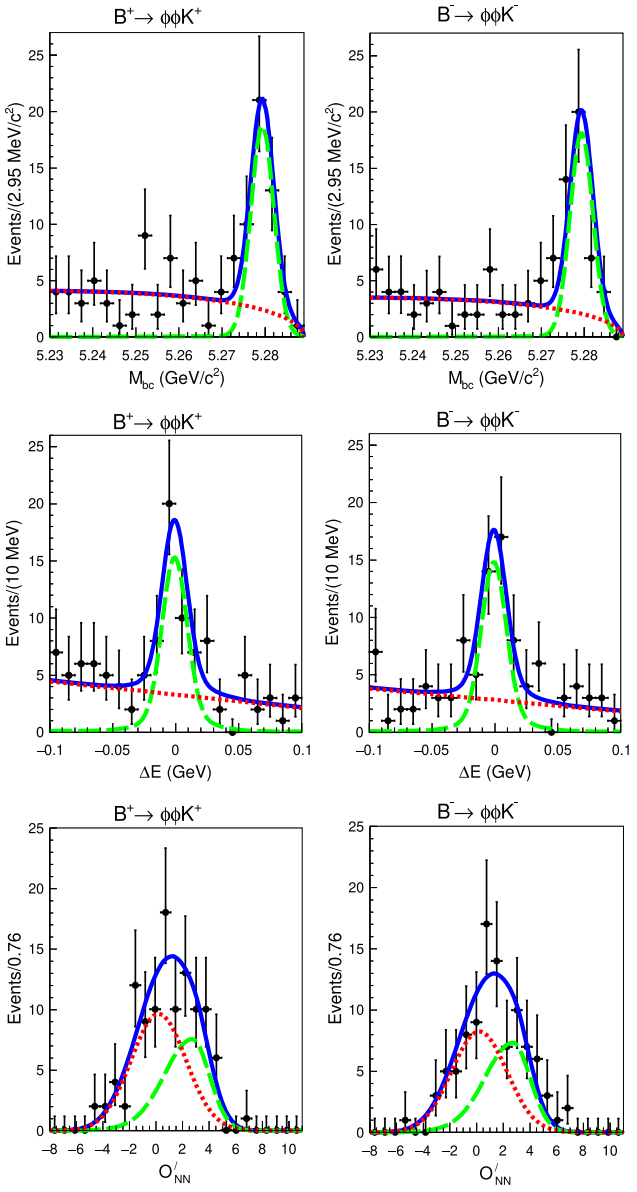

FIG. 2. Projections of $B^{\pm} \to \phi\phi K^{\pm}$ candidate events onto (top) $M_{\rm bc}$, (middle) ΔE, and (bottom) $O'_{\rm NN}$. Black points with error bars are the data, solid blue curves are the total PDF, dashed green curves are the signal component, and dotted red curves are the combined $q\bar{q}$ and $B\bar{B}$ background components.

by the sum of ($M_{K_1K2} \in [1.04, 1.2]$ GeV/c^2 and $M_{K_3K4} \in [1.0, 1.04]$ GeV/c^2) and ($M_{K_1K2} \in [1.0, 1.04]$ GeV/c^2 and $M_{K_3K4} \in [1.04, 1.2]$ GeV/c^2), and SB2 is denoted by $M_{K_1K2} \in [1.04, 1.2]$ GeV/c^2 and $M_{K_3K4} \in [1.04, 1.2]$ GeV/c^2. In Fig. 5 we plot the distribution of data events in the $M_{K_1K_2}$ vs $M_{K_3K_4}$ plane showing SR, SB1, and SB2. The resonant $B \to \phi\phi K$ yield in SR is obtained by solving the following three linear equations:

$$N_0 = n_s + r_{a0} \times n_a + r_{b0} \times n_b, \tag{6}$$

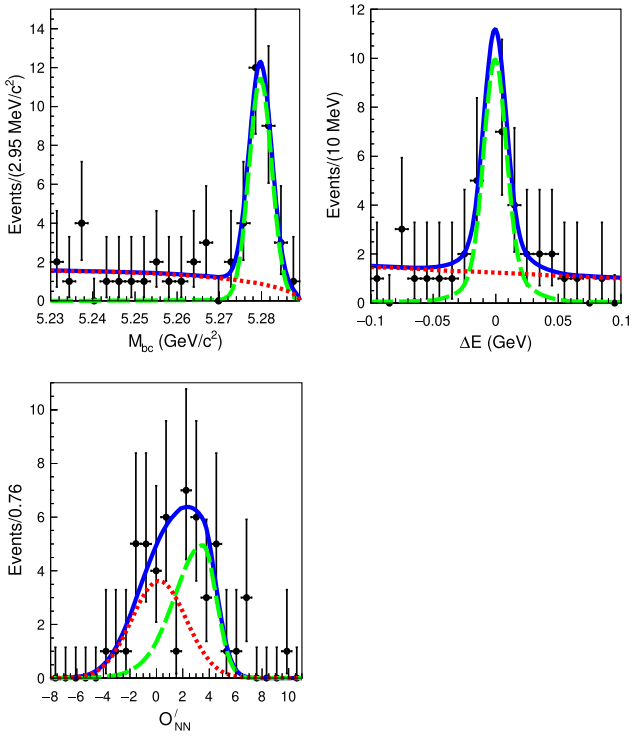

FIG. 3. Projections of $B^0 \to \phi\phi K^0$ candidate events onto (top left) $M_{\rm bc}$, (top right) ΔE, and (bottom) $O'_{\rm NN}$. The legends of the plots are defined in the same manner as in Fig. 2.

$$N_1 = r_{s1} \times n_s + n_a + r_{b1} \times n_b, \tag{7}$$

$$N_2 = r_{s2} \times n_s + r_{a2} \times n_a + n_b, \tag{8}$$

where N_0, N_1, and N_2 are the yields obtained in SR, SB1, and SB2, respectively; n_s, n_a, and n_b are the $B \to \phi\phi K$ yield in SR, $B \to \phi KKK$ yield in SB1, and $B \to KKKK$ yield in SB2, respectively. Lastly, r_{s1} and r_{s2} are the ratios of $B \to \phi\phi K$ yields in SB1 and SB2 to that in SR; r_{a0} and r_{a2} are the ratios of $B \to \phi KKK$ yields in SR and SB2 to

TABLE II. Number of candidate events ($n_{\rm cand}$), detection efficiency (ε), total and resonant signal yield ($n_{\rm sig}$), significance, branching fraction ($\mathcal{B}$) and CP asymmetry ($\mathcal{A}_{CP}$) obtained from a fit to data for $B \to \phi\phi K$ decays below and within the η_c region. Quoted uncertainties are statistical only, and significances defined in the text are given in terms of standard deviations.

	$B^+ \to \phi\phi K^+$	$B^0 \to \phi\phi K^0$	$B^+ \to \phi\phi(\eta_c)K^+$
$n_{\rm cand}$	207	51	84
$\varepsilon(\%)$	12.4	12.0	15.4
Total $n_{\rm sig}$	$85.0^{+10.2}_{-9.5}$	$26.5^{+5.8}_{-5.1}$	$73.2^{+9.0}_{-8.3}$
Significance	14.9	7.2	16.7
Resonant $n_{\rm sig}$	$81.8^{+10.1}_{-9.4}$	$23.7^{+5.7}_{-5.0}$	...
$\mathcal{B}(10^{-6})$	$3.43^{+0.48}_{-0.46}$	$3.02^{+0.75}_{-0.66}$	...
$\mathcal{A}_{CP}$	-0.02 ± 0.11	...	$+0.12 \pm 0.12$

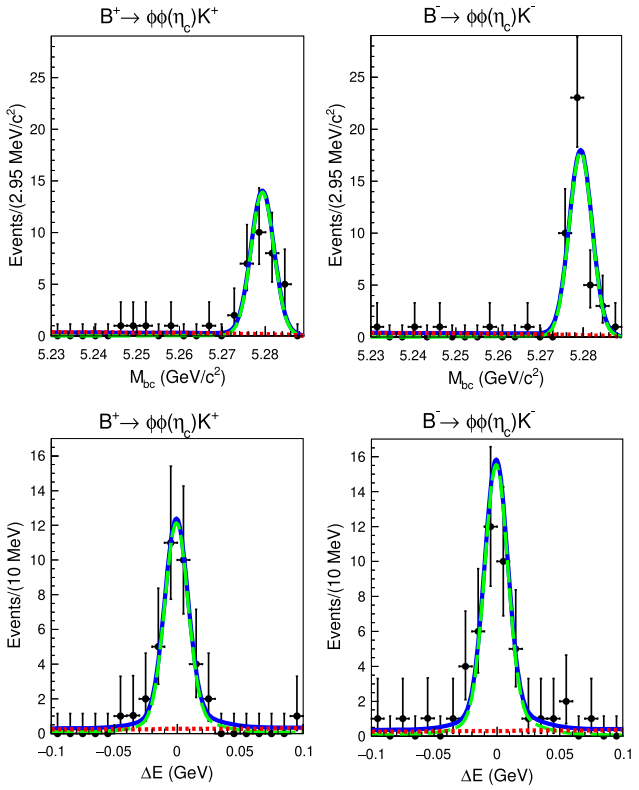

FIG. 4. Projections of $B^{\pm} \to \phi\phi K^{\pm}$ candidate events within the η_c region onto (top) $M_{\rm bc}$ and (bottom) ΔE. The legends of the plots are defined in the same manner as in Fig. 2.

that in SB1; and r_{b0} and r_{b1} are the ratios of $B \to KKKK$ yields in SR and SB1 to that in SB2. All these ratios are obtained from an MC study. We obtain the resonant $B \to \phi\phi K$ yield in SR (n_s) as $81.8^{+10.1}_{-9.4}$ and $23.7^{+5.7}_{-5.0}$ for the charged and neutral mode, respectively. These n_s values are used in the branching fraction calculation of Eq. (5).

The background-subtracted distributions [18] of $m_{\phi\phi}$ and $m_{\phi K}$ obtained for $B^{\pm} \to \phi\phi K^{\pm}$ below the η_c threshold are shown in Fig. 6. These are broadly compatible with the

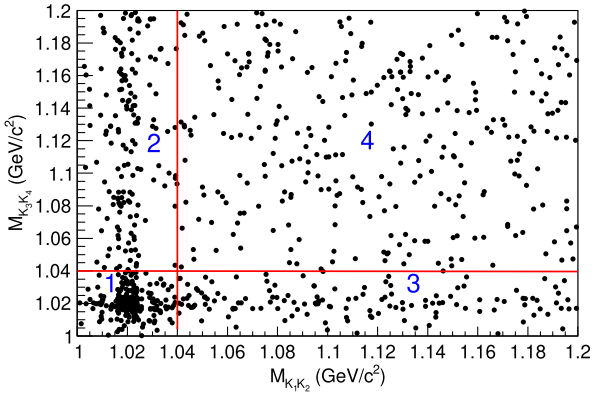

FIG. 5. Distribution of data events in the $M_{K_1K_2}$ vs $M_{K_3K_4}$ plane which shows the M_{KK} signal region (region 1) and two sidebands SB1 (region 2 and 3) and SB2 (region 4).

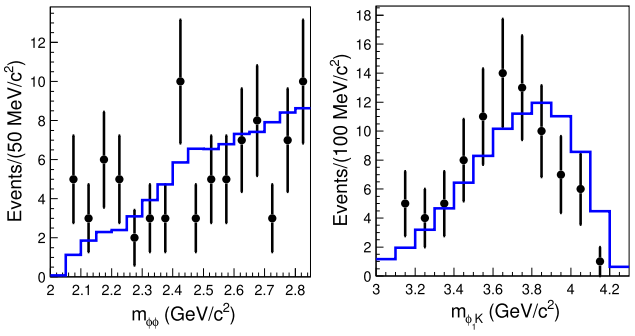

FIG. 6. Background-subtracted signal yield as a function of $m_{\phi\phi}$ (left) and $m_{\phi_1 K}$ (right) for $B^{\pm} \to \phi\phi K^{\pm}$. Black points with error bars are data and solid blue histograms denote the expectation from a phase-space MC sample.

predictions of a three-body phase space MC sample. In particular, we do not find any enhancement in the $m_{\phi\phi}$ spectrum, including the 2.3 GeV$/c^2$ region [3] where a glueball and $X(2350)$ candidates are predicted.

Systematic uncertainties in the branching fraction are listed in Table III. The uncertainties due to PDF shapes are estimated by varying all the fixed shape parameters by their errors. In particular, for fixed signal shape parameters, we vary the data-MC corrections by their uncertainties as determined using the control sample of $B^+ \to D_s^+ \bar{D}^0$ decays. Potential fit bias is checked by performing an ensemble test comprising 1000 pseudoexperiments, where signal is taken from the corresponding MC sample, and the PDF shapes are used to generate background events. We obtain a Gaussian normalized residual distribution of unit width, and add its mean and uncertainty in width in quadrature to calculate the systematic error. Uncertainty due to continuum suppression is obtained with the $B^+ \to D_s^+ \bar{D}^0$ control sample by comparing, between data and simulation, fit results obtained with and without the $O_{\rm NN}$ requirement. A $D^{*+} \to D^0(K^-\pi^+)\pi^+$ control sample is used to determine the systematic uncertainty due to the

TABLE III. Systematic uncertainties (in %) in the branching fractions. Values listed in the top three rows impact the signal yield and are included in the calculation of signal significance.

Source	$B^{\pm} \to \phi\phi K^{\pm}$	$B^0 \to \phi\phi K^0$
Signal PDF	$^{+1.5}_{-1.7}$	$^{+1.3}_{-1.9}$
Background PDF	⋯	$^{+3.0}_{-1.9}$
Fit bias	± 1.7	± 2.0
Efficiency variation	± 2.1	± 2.1
$\mathcal{R}_{K/\pi}$ requirement	± 5.2	± 4.3
$q\bar{q}$ suppression	± 0.5	± 0.5
Track reconstruction	± 1.8	± 1.4
K_S^0 reconstruction	⋯	± 0.9
Number of $B\bar{B}$ events	± 1.4	± 1.4
Total	± 6.5	$^{+6.5}_{-6.3}$

TABLE IV. Systematic uncertainties in $\mathcal{A}_{CP}$.

Source	$B^{\pm} \to \phi\phi K^{\pm}$	$B^{\pm} \to \phi\phi(\eta_c)K^{\pm}$
Detection asymmetry	± 0.008	± 0.008
Signal PDF shape	$^{+0.002}_{-0.003}$	± 0.002
Total	± 0.01	± 0.01

$\mathcal{R}_{K/\pi}$ requirement. We use partially reconstructed $D^{*+} \to D^0(K^0_S\pi^+\pi^-)\pi^+$ decays to assign the systematic uncertainty due to charged-track reconstruction (0.35% per track). The uncertainty due to K^0_S reconstruction is estimated from $D^0 \to K^0_S K^0_S$ decays [19]. We estimate the uncertainty due to efficiency variation across the Dalitz plot by comparing the yield obtained in bins of $m_{\phi\phi}$ and $m_{\phi_1 K}$ between data and phase-space signal MC samples. We fit the background-subtracted $m_{\phi\phi}$ and $m_{\phi_1 K}$ distributions in data (Fig. 6) using a first- and second-order Chebyshev polynomial, respectively. The bin-by-bin scale factors, given by the ratio of signal yields in data and MC events, are propagated to the phase space MC sample. We then calculate the difference in efficiency between reweighted and original MC events. The uncertainties in the polynomial coefficients are also considered in this calculation. The efficiency differences move in both positive and negative directions, with their magnitudes lying in the range 0.7–2.1%. We assign the maximum difference (2.1%) as the systematic uncertainty. The total systematic uncertainty is obtained by adding all the above contributions in quadrature.

We consider two possible sources of systematic uncertainties contributing to $\mathcal{A}_{CP}$, as listed in Table IV. The first is due to the intrinsic detector bias on charged kaon detection and is estimated using $D^+_s \to \phi\pi^+$ and $D^0 \to K^-\pi^+$ decays [20]. The second arises due to the potential variation of the PDF shapes. We calculate its contribution by following a procedure similar to that used in estimating the PDF shape uncertainties in the branching fractions.

In summary, we have measured the branching fractions and CP-violation asymmetries in $B \to \phi\phi K$ decays based on the full $\Upsilon(4S)$ data sample of 772×10^6 $B\bar{B}$ events collected by the Belle detector at the KEKB asymmetric-energy e^+e^- collider. We obtain the branching fraction and CP asymmetry for $B^{\pm} \to \phi\phi K^{\pm}$ below the η_c threshold ($m_{\phi\phi} < 2.85\ \mathrm{GeV}/c^2$) as

$$(3.43^{+0.48}_{-0.46} \pm 0.22) \times 10^{-6} \tag{9}$$

and

$$-0.02 \pm 0.11 \pm 0.01, \tag{10}$$

respectively. We also report the CP-violation asymmetry for $B^{\pm} \to \phi\phi K^{\pm}$ in the η_c region ($m_{\phi\phi} \in [2.94, 3.02]\ \mathrm{GeV}/c^2$) to be

$$+0.12 \pm 0.12 \pm 0.01, \tag{11}$$

consistent with no CP violation. The obtained value of the branching fraction of $B^{\pm} \to \phi\phi K^{\pm}$ decay is consistent with and supersedes our previous result [5]. The measured branching fraction for $B^0 \to \phi\phi K^0$ below the η_c threshold is

$$(3.02^{+0.75}_{-0.66} \pm 0.20) \times 10^{-6}. \tag{12}$$

We find no evidence for glueball production in these decays.

ACKNOWLEDGMENTS

S. M. acknowledges fruitful discussions with S. Mahapatra (Utkal University). We thank the KEKB group for excellent operation of the accelerator; the KEK cryogenics group for efficient solenoid operations; and the KEK computer group, the NII, and PNNL/EMSL for valuable computing and SINET5 network support. We acknowledge support from MEXT, JSPS and Nagoya's TLPRC (Japan); ARC (Australia); FWF (Austria); NSFC and CCEPP (China); MSMT (Czechia); CZF, DFG, EXC153, and VS (Germany); DAE, Project Identification No. RTI 4002, and DST (India); INFN (Italy); MOE, MSIP, NRF, RSRI, FLRFAS project, GSDC of KISTI and KREONET/GLORIAD (Korea); MNiSW and NCN (Poland); MSHE, Agreement 14.W03.31.0026 (Russia); University of Tabuk (Saudi Arabia); ARRS (Slovenia); IKERBASQUE (Spain); SNSF (Switzerland); MOE and MOST (Taiwan); and DOE and NSF (USA).

[1] N. Cabibbo, Phys. Rev. Lett. **10**, 531 (1963); M. Kobayashi and T. Maskawa, Prog. Theor. Phys. **49**, 652 (1973).
[2] M. Hazumi, Phys. Lett. B **583**, 285 (2004).
[3] C. K. Chua, W.-S. Hou, and S.-Y. Tsai, Phys. Lett. B **544**, 139 (2002).
[4] Z. Q. Liu *et al.* (Belle Collaboration), Phys. Rev. Lett. **108**, 232001 (2012).
[5] H. C. Huang *et al.* (Belle Collaboration), Phys. Rev. Lett. **91**, 241802 (2003).
[6] Inclusion of charge-conjugate reactions is implied unless stated otherwise.

[7] S. Fajfer, T. N. Pham, and A. Prapotnik, Phys. Rev. D **69**, 114020 (2004).
[8] C.-H. Chen and H.-N. Li, Phys. Rev. D **70**, 054006 (2004).
[9] J. P. Lees *et al.* (*BABAR* Collaboration), Phys. Rev. D **84**, 012001 (2011).
[10] A. Abashian *et al.* (Belle Collaboration), Nucl. Instrum. Methods Phys. Res., Sect. A **479**, 117 (2002); also see the detector section in J. Brodzicka *et al.*, Prog. Theor. Exp. Phys. **2012**, 04D001 (2012).
[11] S. Kurokawa and E. Kikutani, Nucl. Instrum. Methods Phys. Res., Sect. A **499**, 1 (2003), and other papers included in this Volume; T. Abe *et al.*, Prog. Theor. Exp. Phys. **2013**, 03A001 (2013), and references therein.
[12] P. A. Zyla *et al.* (Particle Data Group), Prog. Theor. Exp. Phys. **2020**, 083C01 (2020).
[13] M. Feindt and U. Kerzel, Nucl. Instrum. Methods Phys. Res., Sect. A **559**, 190 (2006).
[14] S. H. Lee *et al.* (Belle Collaboration), Phys. Rev. Lett. **91**, 261801 (2003).
[15] S. Brandt, C. Peyrou, R. Sosnowski, and A. Wroblewski, Phys. Lett. **12**, 57 (1964); E. Farhi, Phys. Rev. Lett. **39**, 1587 (1977).
[16] D. J. Lange, Nucl. Instrum. Methods Phys. Res., Sect. A **462**, 152 (2001).
[17] H. Albrecht *et al.* (ARGUS Collaboration), Phys. Lett. B **241**, 278 (1990).
[18] M. Pivk and F. R. Le Diberder, Nucl. Instrum. Methods Phys. Res., Sect. A **555**, 356 (2005).
[19] N. Dash *et al.* (Belle Collaboration), Phys. Rev. Lett. **119**, 171801 (2017).
[20] M. Staric *et al.* (Belle Collaboration), Phys. Rev. Lett. **108**, 071801 (2012).